PROCEEDINGS OF SCIENCE

Studies of rare B meson decays with the CMS detector

Xin SHI[*†]
National Taiwan University
E-mail: Xin.Shi@cern.ch

Rare beauty decays are usually an excellent probe to the physics beyond the standard model. Especially those decays, that are proceed through flavor-changing neutral currents, can have the interference from new physics with the loop diagrams. Some of these decays are well predicted by the theory, such as $B_{s,d} \to \mu^+\mu^-$ branching fractions and the $A_{\rm FB}$ of the $B \to K^*\mu^+\mu^-$, are the gold plate searches at the colliders.

XXI International Workshop on Deep-Inelastic Scattering and Related Subjects
22-26 April, 2013
Marseilles, France

[*]Speaker.
[†]On behalf of CMS collaboration

1. Introduction

Rare beauty decays such as $B_{s,d} \to \mu^+\mu^-$ branching fractions and the $A_{\rm FB}$ of the $B \to K^*\mu^+\mu^-$ are well predicted by the Standard Model (SM) theory. New physics beyond the SM can inter through the loop diagram by the flavor-changing neutral currents (FCNC). Thus, looking through the enhancement of such channels are gold plates searches at the colliders.

The CMS detector [3] is a general purpose detector at the LHC. It's inner tracker consists of silicon pixel and silicon strip layers. Muons are measured by drift tubes (DT), cathode strip chambers (CSC) and resistive plate chambers (RPC). The dimuon mass resolution is less than 1%, which makes it a powerful tool for B-physics study.

2. Angular analysis and branching ratio measurement of the decay $B^0 \to K^{*0}\mu^+\mu^-$

2.1 Motivation

The $b \to s\ l^+l^-$ transition is a FCNC process. The amplitudes may interfere with non-SM particle contributions see in Figure 1. The decay is fully described with three angles as shown in Figure 2 and well predicted [1] as shown Figure 3.

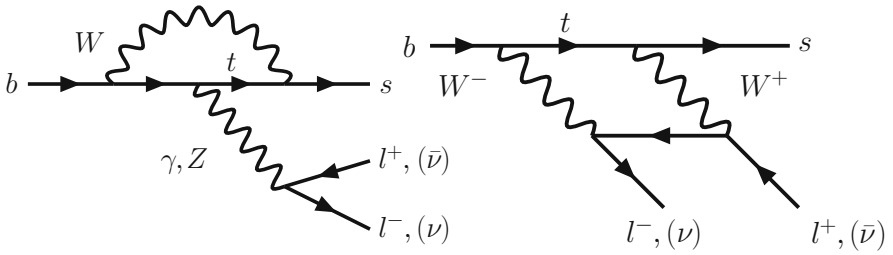

Figure 1: The Feynman diagram of the FCNC process.

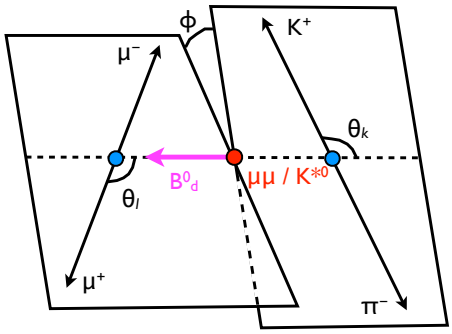

Figure 2: The decay angles of $B \to K^*\mu^+\mu^-$.

$B \to K^*\mu^+\mu^-$ decay is well described with theory. Example of angular observables theoretically predicted with relatively small uncertainties at low q^2 $\mu^+\mu^-$ forward-backward asymmetry ($A_{\rm FB}$).

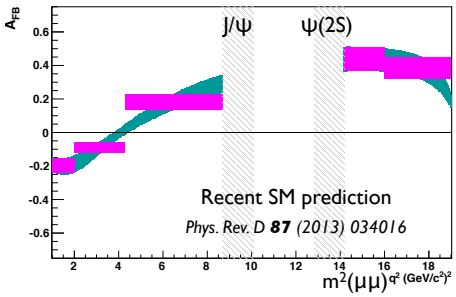

Figure 3: Theory predictions for the forward-backward asymmetry as function of q^2.

2.2 Event Selection and signal yields in q^2 bins

The selection is performed with respect to the ~ 5.2 fb^{-1} data collected by CMS detector during 2011. For dimuon trigger selection: dimuon vertex $L/\sigma > 3$ in transverse plane, the invariant mass of dimuon is between 1 and 4.8 GeV/c^2; dimuon p_{T} from 6.5 GeV/c up to 6.9 GeV/c, single p_{T} of muon larger than 3 GeV/c ($\sim$5 GeV/c with different trigger), dimuon vertex confidence level (CL) larger than 5%, 15% (with different trigger).

Choose two oppositely charged hadrons: require no overlap with muons, $p_{\mathrm{T}}(\mathrm{h}) > 0.75$ GeV/c, Distance closest approach over sigma > 1.3, $K\pi$ invariant mass differs the PDG value of K^{*0} within 80 MeV/c^2.

For the B^0 candidate, we choose the B^0 vertex CL > 9%, B^0 vertex $L/\sigma > 12$ (transverse), $\cos\alpha > 0.9994$ where alpha angle in transverse plane between B^0 momentum and line-of-flight.

The CP state are assigned according to the K^{*0} and $\overline{K^{*0}}$ masses based on the closest distance from PDG. We reject event if both K^{*0} and $\overline{K^{*0}}$ masses are within 50 MeV/c^2 of PDG mass ($\sim 1\Gamma$)

The signal yields are shown in Figure 4, where the solid line are composed of signal, combinatorial background, and peaking background which comes from the feed-through from resonant channels.

The q^2 bins has been chosen according to Table 1.

q2 bin index	mass range (GeV/c2)2
0	1-2
1	2 - 4.3
2	4.3 - 8.68
4	10.09 - 12.86
6	14.18 - 16
7	16 - 19

Table 1: Definition of the q^2 bins. Bin 3 and 5 are J/ψ and $\psi(2S)$ regions respectively.

2.3 Fit strategy and validation with control channels

We use unbinned maximum likelihood fits for B^0 mass, θ_k and θ_l for each q^2 bin to extract $F_{\mathrm{L}}(q^2)$ and $A_{\mathrm{FB}}(q^2)$ as shown in Eq. 2.1 from Ref.[2].

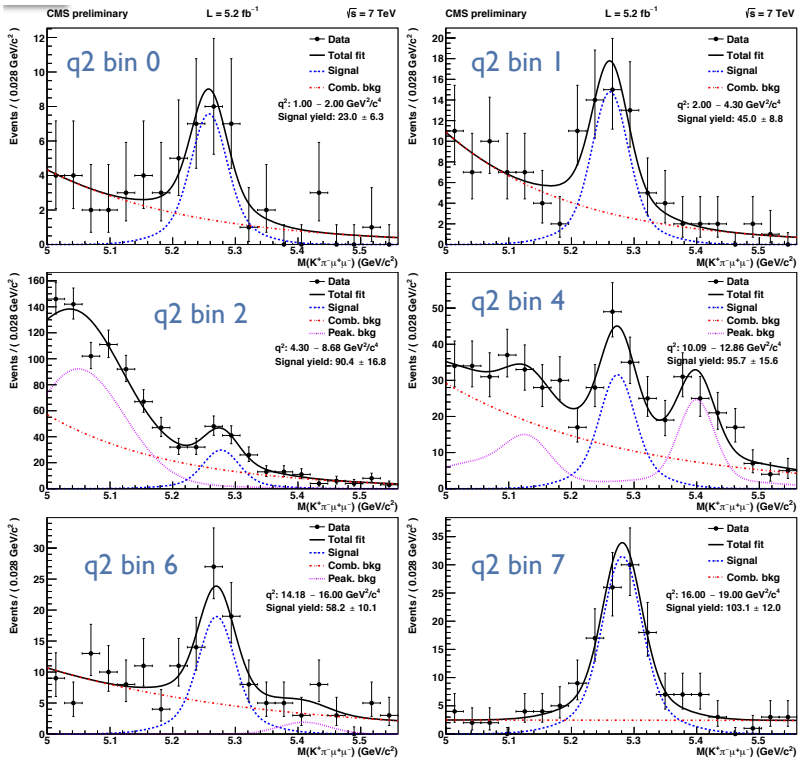

Figure 4: Signal yields in different q^2 bins. Where the blue stands for signal, red for combinatorial background and magenta for peaking background.

$$\begin{aligned}\frac{1}{\Gamma}\frac{\mathrm{d}^3\Gamma}{\mathrm{d}\cos\theta_k \mathrm{d}\cos\theta_l \mathrm{d}q^2} &= \frac{9}{16}((\frac{2}{3}F_S + \frac{4}{3}A_S\cos\theta_k)(1-\cos^2\theta_l) \\ &+ (1-F_S)(2F_{\mathrm{L}}\cos^2\theta_k(1-\cos^2\theta_l) \\ &+ \frac{1}{2}(1-F_{\mathrm{L}})(1-\cos^2\theta_k)(1+\cos^2\theta_l) \\ &+ \frac{4}{3}A_{\mathrm{FB}}(1-\cos^2\theta_k)\cos\theta_l))).\end{aligned} \tag{2.1}$$

where P and S wave of $K\pi$ and their interference are also considered in the PDF, and fit from $B^0 \to K^{*0}J/\psi$, F_S is fraction of S-wave, A_S is the interference between S and P-waves.

Using previous fit results, then fit the B^0 invariant mass to extract the branching fraction: dBF/dq^2,

$$\frac{dBF}{dq^2} = \frac{Y_S \varepsilon_N BF(B^0 \to K^{*0}J/\psi)}{Y_S \varepsilon_S dq^2} \tag{2.2}$$

where Y_S, Y_N are yields of the signal and normalization channel, ε_S, ε_N are efficiency of the signal and normalization channel.

The PDF is composed of Signal: data yield, lineshape of mass (double Gaussian from MC) and decay rate. Combinatorial background: data yield, lineshape of mass (exponential) and angles (polynomials from MC).

$$\begin{aligned} \text{p.d.f.}(m,\theta_k,\theta_l) &= Y_{Si}\, S_i^M(m)\cdot S_i^A(\theta_k,\theta_l)\cdot \varepsilon_i(\theta_k,\theta_l) \\ &+ Y_{Bi}^c B_i^{Mc}(m)\cdot B_i^{\theta_k c}(\theta_k)\cdot B_i^{\theta_l c}(\theta_l) \\ &+ Y_{Bi}^p B_i^{Mp}(m)\cdot B_i^{\theta_k p}(\theta_k)\cdot B_i^{\theta_l p}(\theta_l). \end{aligned} \tag{2.3}$$

where index i runs over q^2 bins.

The fitting procedure is validated with control channels, we can see the good agreement with expected values.

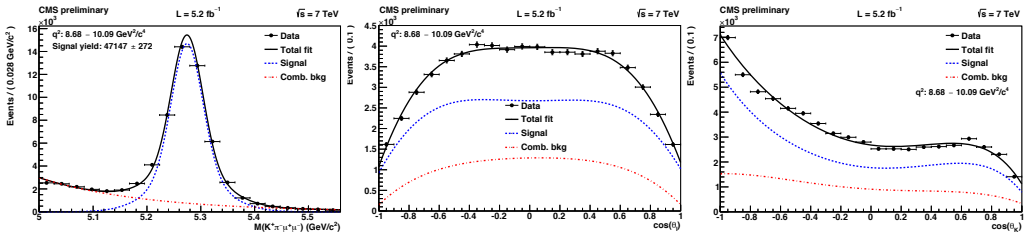

Figure 5: Validation with control channels.

The results of the measurements for the control channel J/ψ are:

- $F_{\mathrm{L}} = 0.554 \pm 0.004(\text{stat})$, compatible with the PDG value of 0.570 ± 0.008;
- $A_{\mathrm{FB}} = -0.004 \pm 0.004(\text{stat})$, compatible with zero.

while for the control channel $\psi(2S)$ are:

- $F_{\mathrm{L}} = 0.509 \pm 0.016(\text{stat})$, compatible with the PDG value of 0.46 ± 0.04.
- $A_{\mathrm{FB}} = 0.013 \pm 0.014(\text{stat})$, compatible with zero.

2.4 Systematic uncertainties and fitting results

Various systematic uncertainties have been considered, the values for the F_{L}, A_{FB} and dBF/dq^2 are listed in the Table 2. The fitting results for the three quantities according to the q^2 bins are shown in Figure 6.

To compare with the theories, a special q^2 bin combines bin 1 to 6 has been calculated as shown in figure. The results to compare with the theory can be shown in Table 3. The results can be also compared with other experiments as shown in Figure 8.

Sources of systematic uncertainty	$F_{\rm L}$	$A_{\rm FB}$	dBF/dq^2
Potential bias from fit ingredients	0	0-0.017	0-7.1%
Test of $\frac{\Gamma(B^0\to K^{*0}J/\psi)}{\Gamma(B^0\to K^{*0}\psi(2S))}$	0	0	14.3%
Potential bias from fit algorithm (toy MC)	0.004-0.040	0.012-0.077	0-2.7%
Incorrect CP assignment of decay	0.002-0.006	0.002-0.006	0%
Effect of $K\pi$ S-wave contribution	0.005-0.023	0.006-0.014	5%
Peaking background mass shape	0-0.026	0-0.008	0-15.2 %
Combinatorial background shape vs. $\cos(\theta_{k/l})$	0.003-0.179	0.004-0.161	0-3.3%
Angular resolution	0-0.019	0	0
Signal mass shape	0	0	0.9 %
Statistical uncertainty of simulated events	0.005-0.007	0.003-0.005	1%
Total systematic uncertainty	0.027-0.185	0.018-0.179	15.5-21.5%

Table 2: Systematic uncertainties.

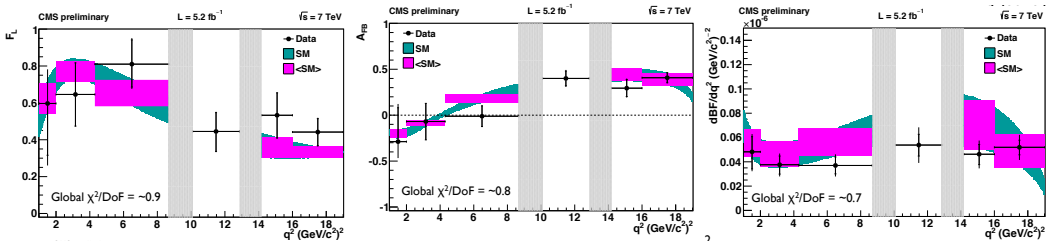

Figure 6: Fitting results for $F_{\rm L}$, $A_{\rm FB}$, and dB/dq^2. Error bars with edges: statistical uncertainty, edges-less error bars: total uncertainty. Purple region: standard model properly averaged over the bin [1].

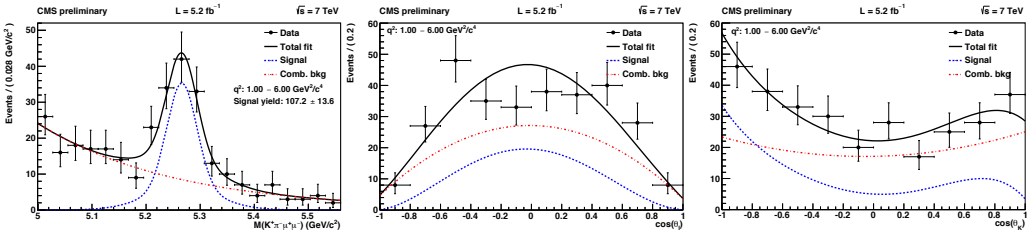

Figure 7: Special q^2 combines bin 1 to 6.

Variables	CMS measurements	SM predictions [1]
$F_{\rm L}$	$0.68 \pm 0.10 \pm 0.02$	$0.74^{+0.06}_{-0.07}$
$A_{\rm FB}$	-0.07 $\pm$ 0.12 $\pm$ 0.01	-0.04 $\pm$ 0.03
dBF/dq^2	$(4.4 \pm 0.6 \pm 0.7) \times 10^{-8} c^4/GeV^2$	$4.9^{+1.0}_{-1.1} \times 10^{-8} c^4/GeV^2$

Table 3: Comparison of q^2 bins from 1 to 6 has been with SM predictions, where the first uncertainty is statistical and second is systematic.

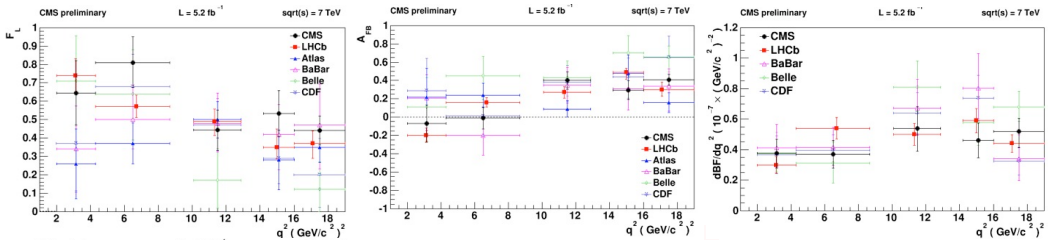

Figure 8: Comparison with other experiments: BaBar: Lake Louise Winter Institute, 2012; Belle: Phys. Rev. Lett. 103(2009) 171801; CDF: Phys. Rev. Let. 108 (2012) 081807; LHCb: Phys. Rev. Lett. 108 (2012) 181806; ATLAS: Beauty 2013.

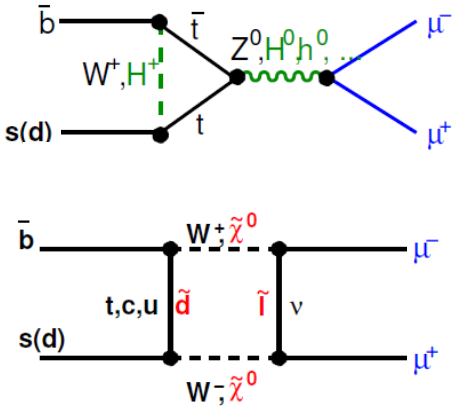

Figure 9: Feynman diagrams of the possible contributions from the new physics.

3. Search for B_s and B^0 decay to dimuons

3.1 Motivation

B_s and B^0 decay to dimuons are doubly suppressed in the SM (FCNC, helicity and Cabibbo suppression) and are well predicted in theory [4].

$$BF(B_s^0 \to \mu^+\mu^-)_{SM} = (3.2 \pm 0.2) \times 10^{-9} \tag{3.1}$$

$$BF(B^0 \to \mu^+\mu^-)_{SM} = (1.0 \pm 0.1) \times 10^{-10} \tag{3.2}$$

They are sensitive to new physics [5]:

$$\frac{BF(B_s^0 \to \mu^+\mu^-)_{CMSSM}}{BF(B_s^0 \to \mu^+\mu^-)_{SM}} \approx 1.2^{+0.8}_{-0.2} \tag{3.3}$$

where CMSSM stands for Constrained Minimal Supersymmetric extension of the Standard Model [6].

$$\frac{BF(B_s^0 \to \mu^+\mu^-)_{NUHM1}}{BF(B_s^0 \to \mu^+\mu^-)_{SM}} \approx 1.9^{+1.0}_{-0.9} \tag{3.4}$$

where NUHM1 stands for Non-Universal Higgs Mass 1 model [7].

3.2 Analysis technique and results

A blind analysis is performed and with $B^+ \to J/\psi K^+$ as normalization channel to remove uncertainties on luminosity and σ_{bb}. It also helps to reduce the systematic uncertainty in BR ratio.

$$BF(B_s^0 \to \mu^+\mu^-) = \frac{N_S}{N_{obs}^{B^+}} \frac{f_u}{f_s} \frac{\varepsilon_{tot}^{B^+}}{\varepsilon_{tot}} \mathscr{B}(B^+). \tag{3.5}$$

The main backgrounds are: collimated muons from two semileptonic B decays (gluon splitting); one muon from semileptonic B decay and one mis-identified hadron, rare decays; and peaking (e.g. $B_s \to K^+K^-$) Non-peaking (e.g. $B_s \to K^+\mu^-\nu$).

Variables used in selection are: muon and dimuon p_{T}, vertex χ^2 probability, pointing angle, impact parameter and flight length significance, dimuon isolation in the cone around the B direction.

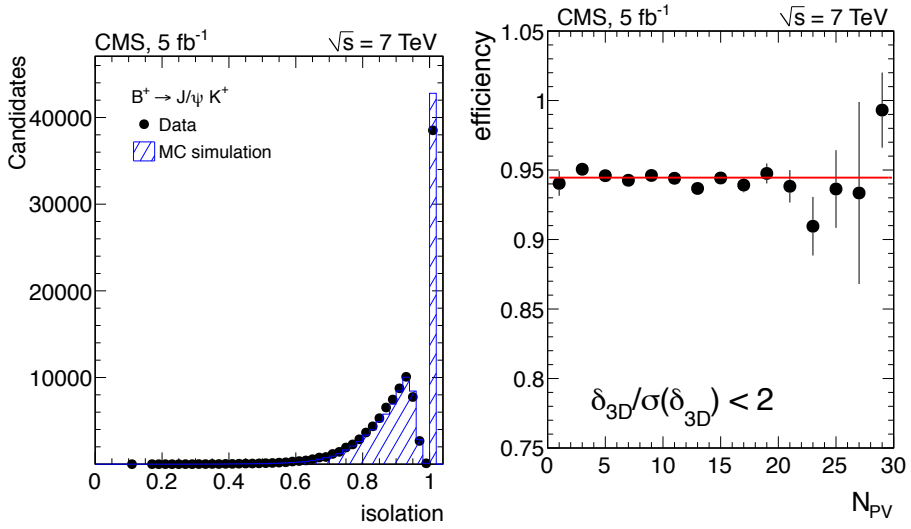

Figure 10: Example variables used in selection.

Cut optimization and count in B^0 and B_s mass windows are done by cheking the robustness against pile-up variations. Mass side-bands for expected background estimation, efficiency ratios from MC and checked in data "tag-and-probe" method and $B_s \to J/\psi\phi$ control sample.

The normalization N_{norm} from invariant mass fit to $B^+ \to J/\psi K^+$ sample. Combinatorial background from dimuon mass side-band interpolation assuming flat distribution. Peaking background shapes are obtained from MC.

The results are shown in Table 4. The expected upper limits and observed upper limits are shown in Table 5.

4. Summary

First result from the angular analysis and differential branching fraction of the decay $B^0 \to$

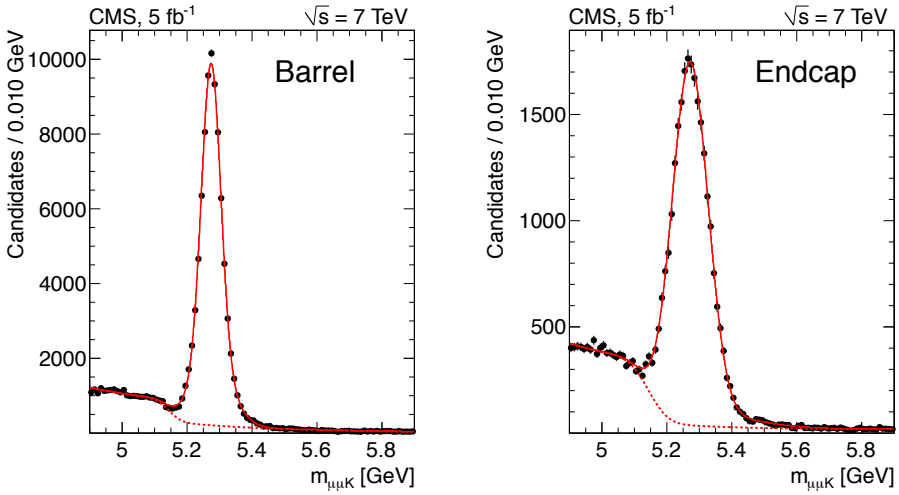

Figure 11: N_{norm} from invariant mass fit to $B^+ \to J/\psi K^+$ sample.

Variable	$B^0 \to \mu^+\mu^-$ Barrel	$B_s^0 \to \mu^+\mu^-$ Barrel	$B^0 \to \mu^+\mu^-$ Endcap	$B_s^0 \to \mu^+\mu^-$ Endcap
ε_{tot}	0.0029 ± 0.0002	0.0029 ± 0.0002	0.0016 ± 0.0002	0.0016 ± 0.0002
$N^{\text{exp}}_{\text{signal}}$	0.24 ± 0.02	2.70 ± 0.41	0.10 ± 0.01	1.23 ± 0.18
$N^{\text{exp}}_{\text{peak}}$	0.33 ± 0.07	0.18 ± 0.06	0.15 ± 0.03	0.08 ± 0.02
$N^{\text{exp}}_{\text{comb}}$	0.40 ± 0.34	0.59 ± 0.50	0.76 ± 0.35	1.14 ± 0.53
$N^{\text{exp}}_{\text{total}}$	0.97 ± 0.35	3.47 ± 0.65	1.01 ± 0.35	2.45 ± 0.56
N_{obs}	2	2	0	4

Table 4: Results.

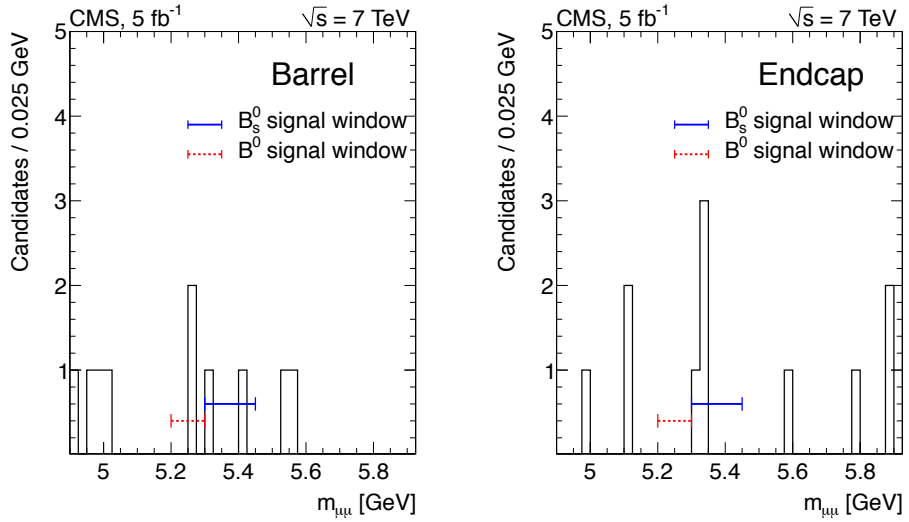

Figure 12: Results in Barrel and Endcap region

Channel	Expected ULs	Observed ULs
BR ($B_s \to \mu^+\mu^-$)	$< 8.4 \times 10^{-9}$ @ 95% CL	$< 7.7 \times 10^{-9}$ @ 95% CL
BR ($B_d \to \mu^+\mu^-$)	$< 1.6 \times 10^{-9}$ @ 95% CL	$< 1.8 \times 10^{-9}$ @ 95% CL

Table 5: Final Results.

$K^{*0}\mu^+\mu^-$. Stringent constraints on new physics with the search for B_s and B^0 decay to dimuons. Updates with the full 2012 data are expected soon.

References

[1] *Phys. Rev. D* **87** (2013) 034016

[2] *JHEP* **03** (2013) 027

[3] Chatrchyan S *et al.* (CMS Collaboration) 2008 *JINST* **3** S08004

[4] *Phys. Lett. B* **694** (2010) 402

[5] *Phys. Lett. B* **639** (2006) 499

[6] *Phys. Rev. D* **47** (1993) 376

[7] *Phys. Rev. D* **71** (2005) 095008